



# Diagnosing evapotranspiration responses to water deficit across biomes using deep learning

## Journal Article

### Author(s):

Giardina, Francesco ; Gentine, Pierre; Konings, Alexandra G.; Seneviratne, Sonia I. ; Stocker, Benjamin D.

### Publication date:

2023-11

### Permanent link:

<https://doi.org/10.3929/ethz-b-000628261>

### Rights / license:

[Creative Commons Attribution 4.0 International](#)

### Originally published in:

New Phytologist 240(3), <https://doi.org/10.1111/nph.19197>

### Funding acknowledgement:

181115 - next-generation Modelling of the biosphere - Including New Data streams and optimality approaches (SNF)

# Diagnosing evapotranspiration responses to water deficit across biomes using deep learning

Francesco Giardina<sup>1,2</sup> , Pierre Gentine<sup>3,4</sup> , Alexandra G. Konings<sup>5</sup> , Sonia I. Seneviratne<sup>6</sup>  and Benjamin D. Stocker<sup>1,2,7,8</sup> 

<sup>1</sup>Institute of Agricultural Sciences, Department of Environmental Systems Science, ETH Zürich, Zürich, CH-8092, Switzerland; <sup>2</sup>Swiss Federal Institute for Forest, Snow and Landscape Research WSL, Birmensdorf, CH-8903, Switzerland; <sup>3</sup>Department of Earth and Environmental Engineering, Columbia University, New York, NY 10027, USA; <sup>4</sup>Center for Learning the Earth with Artificial Intelligence and Physics (LEAP), Columbia University, New York, NY 10027, USA; <sup>5</sup>Department of Earth System Science, Stanford University, Stanford, CA 94305, USA; <sup>6</sup>Institute for Atmospheric and Climate Science, Department of Environmental Systems Science, ETH Zurich, Zürich, CH-8092, Switzerland; <sup>7</sup>Institute of Geography, University of Bern, Hallerstrasse 12, Bern, 3012, Switzerland; <sup>8</sup>Oeschger Centre for Climate Change Research, University of Bern, Falkenplatz 16, Bern, 3012, Switzerland

## Summary

Author for correspondence:

Francesco Giardina

Email: [francesco.giardina@alumni.epfl.ch](mailto:francesco.giardina@alumni.epfl.ch)

Received: 21 April 2023

Accepted: 23 July 2023

*New Phytologist* (2023) **240**: 968–983

doi: 10.1111/nph.19197

**Key words:** climate change, deep learning, drought, groundwater, rock moisture, root zone water storage capacity, soil moisture, vapor pressure deficit.

- Accounting for water limitation is key to determining vegetation sensitivity to drought. Quantifying water limitation effects on evapotranspiration (ET) is challenged by the heterogeneity of vegetation types, climate zones and vertically along the rooting zone.
- Here, we train deep neural networks using flux measurements to study ET responses to progressing drought conditions. We determine a water stress factor (fET) that isolates ET reductions from effects of atmospheric aridity and other covarying drivers. We regress fET against the cumulative water deficit, which reveals the control of whole-column moisture availability.
- We find a variety of ET responses to water stress. Responses range from rapid declines of fET to 10% of its water-unlimited rate at several savannah and grassland sites, to mild fET reductions in most forests, despite substantial water deficits. Most sensitive responses are found at the most arid and warm sites.
- A combination of regulation of stomatal and hydraulic conductance and access to below-ground water reservoirs, whether in groundwater or deep soil moisture, could explain the different behaviors observed across sites. This variety of responses is not captured by a standard land surface model, likely reflecting simplifications in its representation of belowground water storage.

## Introduction

Water availability controls evapotranspiration (ET) over most of the vegetated land surface (Beer *et al.*, 2010; Schwalm *et al.*, 2010; Seneviratne *et al.*, 2010; Ahlström *et al.*, 2015). As droughts may become more severe and frequent in the future (Seneviratne *et al.*, 2021), it is crucial to understand how plant function links ecosystem ET and water limitation. Quantifying water limitation effects on ET is challenged by the heterogeneity of the soil and bedrock structure, both vertically along the rooting zone and laterally across the landscape (Thompson *et al.*, 2011; Gao *et al.*, 2014; Dralle *et al.*, 2020). Understanding ET responses to drought will become increasingly important in the future, given the extensive transition from energy-limited to water-limited regimes that is occurring with climate change (Seneviratne *et al.*, 2006, 2010; Denissen *et al.*, 2022).

The root zone water storage capacity ( $S_0$ ) defines the maximum amount of soil moisture that plants can access for transpiration (and thus, the amount of soil moisture that affects ET). A large  $S_0$  has been linked to a higher plant resistance to drought,

sustained ET, deeper roots and persistent vegetation cover during rain-free periods (Teuling *et al.*, 2006; Gao *et al.*, 2014; Stocker *et al.*, 2023). Recent studies have identified locally important contributions to  $S_0$  by water reservoirs below the soil layer, such as in fractured bedrock (Rempe & Dietrich, 2018; Dawson *et al.*, 2020; McCormick *et al.*, 2021) or groundwater (Thompson *et al.*, 2011; Hain *et al.*, 2015; Fan *et al.*, 2017). In settings with pronounced topographical gradients or groundwater convergence, water-saturated zones can be within the reach of roots (Fan *et al.*, 2013, 2017). This implies large variations in plant available water at small spatial scales, as also suggested by inverse modelling (Hain *et al.*, 2015; Fan *et al.*, 2017). However, direct observations of these effects are sparse and limited to a small number of individual field sites (Thompson *et al.*, 2011; Rempe & Dietrich, 2018).

Another mechanism put in place by plants to reduce water loss during drought is to rely on a very resistant xylem (Plaut *et al.*, 2012; Mackay *et al.*, 2015). Some species are able to withstand water stress conditions thanks to xylem structural features that allow them to avoid embolism and to sustain ET during

drought (Meinzer *et al.*, 2009). These plants have larger hydraulic safety margins and are thus more drought-tolerant (McDowell *et al.*, 2008). This is in contrast with other plant species that rely on the release of stored water to maintain hydraulic safety (Meinzer *et al.*, 2009).

The role of water limitation on ET and its importance for ecosystem fluxes across vegetation types and climate zones have remained poorly understood. This is partly due to challenges in separating partial effects of water stress on ecosystem fluxes from multiple covarying drivers. In particular, soil moisture and vapor pressure deficit (VPD) jointly affect ET, but tend to covary (Novick *et al.*, 2016; Giardina *et al.*, 2018; Zhou *et al.*, 2019; L. Liu *et al.*, 2020; Y. Liu *et al.*, 2020). The soil moisture-VPD coupling is generally observed as a result of land-atmosphere feedbacks under relatively dry conditions (Seneviratne *et al.*, 2010; L. Liu *et al.*, 2020), but this correlation can fade under very dry or humid conditions (Ruddell & Kumar, 2009). This limits what can be inferred from flux measurements and whether generalizations can be found to inform models across a wide range of conditions.

The complexity of plant responses to water deficit contrasts with its representation in land surface models (LSMs; Fan *et al.*, 2019). With a few exceptions (Fan *et al.*, 2007; Miguez-Macho *et al.*, 2007; Swenson *et al.*, 2019), LSMs represent the land surface as a flat surface (Prentice *et al.*, 2015; Fan *et al.*, 2019), assume free drainage from the bottom soil layer, which prevents the formation of water-saturated zones (Liang *et al.*, 1994; Schlemmer *et al.*, 2018), and do not account for the variety of bedrock lithology and its role as a moisture storage component (McCormick *et al.*, 2021). Some LSMs do not accurately consider the effects of drought on phenology and the seasonal variation in leaf area index (LAI), especially in drought-deciduous regions of the world (Dahlin *et al.*, 2015). Spatial variations of  $S_0$  are typically represented in models based on variations in soil type and in plant rooting depth that are assumed to be fixed and assigned to plant functional types (PFTs; Drewniak, 2019; Tumber-Dávila *et al.*, 2022). These simplifications ignore spatial heterogeneity in plant hydraulics and water stress effects on vegetation, which affects the accuracy at predicting water limitation effects on ET, particularly under drought conditions (Zhang *et al.*, 2016; Green *et al.*, 2017; Kennedy *et al.*, 2019; Stocker *et al.*, 2019). This highlights the need to develop observational benchmarks focusing on the role of water limitation, separated from atmospheric aridity and other covarying drivers (Novick *et al.*, 2016; Giardina *et al.*, 2018; Zhou *et al.*, 2019), for reliable ET modelling.

Here, using site-specific deep neural network (DNN) models, we estimate the fractional reduction in evapotranspiration (fET) at eddy-covariance sites compared with its potential rate. We use 88 000 site days of ecosystem-scale ET measurements, complemented by meteorological measurements, multiple soil moisture datasets and a remotely sensed greenness index. Our method isolates the control of water availability on ET, factoring out effects of VPD and other drivers, that is, vegetation greenness, air temperature and net radiation ( $R_n$ ). We then evaluate fET reductions during drought by regressing it against the cumulative water

deficit (CWD, the cumulative difference between observed ET and precipitation). In contrast to evaluating fET against surface soil moisture, assessment against CWD reveals patterns of water stress effects resulting from whole-column water depletion. We used these analyses to test the following hypotheses: an increasing CWD generally reduces fET across sites; deep moisture storage is important in sustaining ET during prolonged dry periods at some sites, and its signal can be detected in flux-tower measurements, using the fET index; and LSMs underestimate the diversity of fET-CWD relations across sites due to neglected small-scale heterogeneity in plant available water.

## Materials and Methods

### Overview

We started by estimating potential and actual evapotranspiration (PET and ET, respectively) across a large set of sites. PET is defined here as equal to ET in the absence of water limitations, that is, ET at its water-unlimited rate (see the [Estimating potential ET](#) section). For each site, we defined two separate DNN models:  $DNN_{PET}$  and  $DNN_{ET}$ , respectively. Section 3 of Supporting Information Methods S1 contains a detailed description of the tuning of the hyperparameters of the DNNs. The key difference between  $DNN_{PET}$  and  $DNN_{ET}$  is that  $DNN_{PET}$  was trained using data from days with high soil moisture only, whereas  $DNN_{ET}$  was trained using all available data (see the [Estimating potential ET](#) section). We used either observational soil moisture from FLUXNET2015 or modelled soil moisture from a bucket-type soil water balance model (Davis *et al.*, 2017). We preferred modelled data for the many sites where the quality of the observational data was poor, as described in the [Soil moisture data](#) section. We defined a normalized measure of moisture limitation effects on ET (referred to as 'fET') by dividing the neural network estimate of ET ( $ET_{NN}$ ) by the neural network estimate of PET ( $PET_{NN}$ ). Here, we identify 'droughts' by the effects of water balance deficits on vegetation activity (Seneviratne *et al.*, 2021). We thus analyzed how fET evolves with increasing water stress by regressing it against the observed CWD. We grouped sites based on their fET-CWD relationship and analyzed how the site groups vary with soil texture, vegetation classes, moisture index, topographical context of the site, mean annual precipitation and mean annual temperature (MAT) within each group.

### Data

All analyses were performed using R Statistical Software (R Core Team, 2023). We extensively made use of the 'TIDYVERSE' R package to process our data (Wickham *et al.*, 2019). To see the entirety of the R packages used in this study, please refer to our published repository on GitHub and Zenodo.

**Eddy-covariance data** Half-hourly data were downloaded from the FLUXNET2015 website and filtered to keep only measured values (\*\_QC = 0) or values gap-filled with high confidence

(\*\_QC = 1; Pastorello *et al.*, 2020). The latent heat flux was converted from energy units ( $\text{W m}^{-2}$ ) to mass units ( $\text{mm d}^{-1}$ ) by multiplying it by the latent heat of vaporization ( $\text{J kg}^{-1}$ ) as a function of air temperature, using the R package 'BIGLEAF' (Knauer *et al.*, 2018).

To reduce biases in ET predictions, we applied additional filters to the data, as described in Section 1 of Methods S1. Half-hourly data were aggregated into daily data to reduce noise and to avoid the ET-VPD hysteresis effect, observed at sub-daily timescales (Zhang *et al.*, 2014). We only retained daily estimates with at least eight measured half-hourly points, as in Li *et al.* (2019). While aggregating to the daily level, the daily mean was calculated for all variables, except for VPD (for which we calculated the daily maximum), and for ET and precipitation (for which we used the daily sum).

The evaporative fraction (EF), which was used as a consistency check on fET values in our analysis, was calculated using daily aggregates as  $\text{EF} = \frac{\text{latent heat flux}}{R_n}$ .

**Soil moisture data** When possible, we used observational soil moisture data from the FLUXNET2015 dataset. To be consistent across all sites, we only used soil moisture data from the uppermost layer (typically measured within 0–15 cm below-ground), as multiple depths were available only for a very limited number of sites (Pastorello *et al.*, 2020). For many FLUXNET2015 sites, we found that observational soil moisture data were unavailable, incomplete or inconsistent with ET observations, as described in Section 1 of Methods S1. For these sites, we simulated soil moisture with SPLASH, a bucket-type soil water balance model (Davis *et al.*, 2017). This model was based on a Priestley–Taylor formulation for ET estimation. We set the water-holding capacity ('bucket depth') to 220 mm (Orth *et al.*, 2013; Davis *et al.*, 2017). Given that we used both modelled soil moisture and observational soil moisture across sites, the variable was normalized between 0 and 1 on a site-by-site basis for better comparison across sites. Using a modelled soil moisture represented a potential source of circularity in our analysis, since we were assuming a water-holding capacity specific to a rooting depth. However, we mostly used soil moisture to separate the training data into 'moist' and 'dry' days (see the **Estimating potential ET** section), so that the exact modelled values should have only a minimal influence on our results. Using modelled soil moisture at sites with good-quality observational data yielded similar results (Fig. S1).

**Greenness data** We downloaded MODIS EVI (MOD13Q1, Collection 5) with the 'MODISTOOLS' R package (Tuck *et al.*, 2014). Images with clouds, snow, ice or shadows were excluded. To get daily values and remove noise, we applied a Savitzky–Golay smoothing filter ('SIGNAL' R package) with a third-order polynomial and a frame length of 31 d.

**GLDAS data** We downloaded precipitation, ET and PET estimates of the GLDAS\_NOAH025\_3H\_2.1 product from the NASA Global Land Data Assimilation System v.2 (GLDAS-2; Rodell *et al.*, 2004; Beaudoin *et al.*, 2020). This product

provides global land surface fluxes computed based on current satellite- and ground-based observational forcing (Ek *et al.*, 2003; Rodell *et al.*, 2004). GLDAS\_NOAH025\_3H\_2.1 is run with Noah land surface model v.3.6, which can be regarded as a standard LSM due to its extensive utilization within the field and its integration as the land component of the operational Global Forecast System model of the National Centers for Environmental Prediction (NCEP; Rodell *et al.*, 2004; Beaudoin *et al.*, 2020). In our analysis, we compared the outputs of our deep-learning models to GLDAS-NOAH to understand how LSM simulations may agree with observations-driven ET responses to water deficit. We provide a more detailed overview of this product in Section 5 of Methods S1, focusing on how it quantifies soil moisture limitation effects on ET.

We referred to ET and PET from this data product as  $\text{ET}_{\text{GLDAS}}$  and  $\text{PET}_{\text{GLDAS}}$ . We defined  $\text{fET}_{\text{GLDAS}} = \text{ET}_{\text{GLDAS}} / \text{PET}_{\text{GLDAS}}$  to compare it with our deep-learning estimate of fET. The data were originally available at a 3 h time resolution and at a grid resolution of  $0.25^\circ \times 0.25^\circ$ . For two sites (IT-Noe and IT-Cpz), it was not possible to extract GLDAS values, as they were too close to the coastline. After extracting the variables at the site level, we calculated daily means.  $\text{PET}_{\text{GLDAS}}$  displays good correlation with *in-situ* measurements, although it was found to be biased high relative to some satellite products (Zhan *et al.*, 2019). For comparison with  $\text{PET}_{\text{NN}}$ ,  $\text{PET}_{\text{GLDAS}}$  was therefore scaled by dividing it by its median value in the lower CWD bin ( $\text{CWD} < 20 \text{ mm}$ ). This way,  $\text{fET}_{\text{GLDAS}}$  was roughly comprised between 0 and 1.

**Soil texture, climate and topography data** We extracted soil texture distribution data at FLUXNET2015 locations from the Regridded Harmonized World Soil Database v.1.2 (Wieder *et al.*, 2014). We used all soil fractions from the topsoil.

To study the role of climate across sites, we downloaded MAT and mean annual precipitation (MAP) from WorldClim v.2.1, available at a 30 arc-second spatial resolution. We extracted MAT and MAP at FLUXNET2015 sites (Fick & Hijmans, 2017).

The moisture index was calculated with FLUXNET2015 data as the ratio of annual precipitation ( $P$ ) over potential evapotranspiration (PET), for all years in which data were available for the respective sites. Precipitation data are from the FLUXNET 2015 Tier 1 dataset; PET was calculated following the Priestley–Taylor equation ( $\text{PET}_{\text{PT}}$ ), as implemented in the SPLASH model (Davis *et al.*, 2017).

To investigate the role of topography across sites, global topographic index (GTI) values were downloaded from a high-resolution dataset (Marthews *et al.*, 2015a,b) and extracted at FLUXNET2015 locations. Compared with other metrics, the GTI calculates the water balance at the landscape scale, taking into account the local slope and the upstream draining area (Marthews *et al.*, 2015a).

## Estimating potential ET

Our approach was based on a published method that separates soil moisture effects on light-use efficiency using FLUXNET2015 data

(Stocker *et al.*, 2018). Here,  $ET_{NN}$  was estimated using observational ET ( $ET_{obs}$ ) as target variable and soil moisture,  $R_n$ , VPD, air temperature ( $T$ ) and the enhanced vegetation index (EVI) as predictors:

$$ET_{NN} = DNN_{ET}(R_n, VPD, T, EVI, \text{soil moisture}) \quad \text{Eqn 1}$$

$PET_{NN}$  was estimated using  $ET_{obs}$  as target variable and again  $R_n$ , VPD,  $T$  and EVI as predictors, but no longer considering soil moisture:

$$PET_{NN} = DNN_{PET}(R_n, VPD, T, EVI) \quad \text{Eqn 2}$$

For this ecological application, the choice of predictors was limited to a small number representing known environmental controls on ET and PET (Maes *et al.*, 2019; Miralles *et al.*, 2019). A larger number of predictors could increase the possibility of having correlated variables that would have a confounding effect, thus negatively affecting the predictive ability of the model outside of the training set. Adding more predictors improved the performance of the model only marginally (Fig. S2), at the cost of a more computational-intensive model.

$PET_{NN}$  was derived by training the model with data from days when soil moisture was relatively high (i.e. above a site-specific threshold) at the specific site ('moist days'). We thus defined  $PET_{NN}$  as a soil-moisture-unlimited ET. By contrast, the model for predicting  $ET_{NN}$  was trained using all data and with soil moisture as an additional predictor. The threshold to divide data into 'moist' and 'dry' days was determined for each site based on  $ET_{obs}$  and  $PET_{NN}$ , as described in Section 2 of Methods S1. By training  $PET_{NN}$  using data with relatively high soil moisture ('moist' days), we might preferentially exploit a region of the dataset with high LAI (e.g. high EVI). However, we found consistent results when plotting the range and distribution of EVI for 'moist' vs 'dry' days separately (Fig. S3). Moreover, even when the seasonality of EVI and  $ET_{obs}$  has relatively low values,  $PET_{NN}$  remains unaffected (Fig. S4). This indicates that our estimation of PET is not influenced by the dependence of EVI on soil moisture.

We derived the water stress factor (fET) as:

$$fET = \frac{ET_{NN}}{PET_{NN}} \quad \text{Eqn 3}$$

Using this index, we quantified the control of water limitation on ET, separated from other predictors (net radiation, VPD, vegetation greenness and air temperature). Even though VPD and soil moisture can be correlated under specific conditions and timescales (Seneviratne *et al.*, 2010; Novick *et al.*, 2016; Sulman *et al.*, 2016), our deep-learning models were trained with a diverse dataset that includes instances where VPD and soil moisture are decoupled, based on a previous publication which served as the foundational basis for the methodology employed in this paper (Stocker *et al.*, 2018). This approach ensures that the models capture the impact of VPD and soil moisture separately at different locations.

Note that although surface soil moisture data is used as input for the deep-learning model, its information is mainly used for discriminating 'moist' (days when  $ET = PET$ ) from 'dry' conditions. fET can thus be interpreted as reflecting water stress in general, potentially also including moisture stored at deeper levels. This relies on the fact that surface soil moisture values are correlated with deeper soil moisture (Salvucci & Entekhabi, 1994; Qiu *et al.*, 2016).

The use of this neural-network-based approach avoided the necessity to determine PET *a priori* based on theoretical estimations that are difficult to parameterize (Maes *et al.*, 2019). Using  $ET_{NN}$  instead of  $ET_{obs}$  in Eqn 3 resulted in less noisy fET estimates, as  $ET_{NN}$  and  $PET_{NN}$  were affected by similar prediction errors, such as a varying flux measurement footprint and incorrect instantaneous energy balance closure. By definition,  $PET_{NN}$  should agree with  $ET_{obs}$  during 'moist days'. On the contrary,  $PET_{NN}$  was expected to overestimate  $ET_{obs}$  during 'dry days', as the former was trained on 'moist days' data only (Fig. S5).

We evaluated  $PET_{NN}$  against an empirical Priestley–Taylor estimate of PET ( $PET_{PT}$ ) obtained from the SPLASH model (Davis *et al.*, 2017) and against a linear model (lm) estimate of PET ( $PET_{lm}$ ). The site-specific linear regression models were defined as  $PET_{lm} = k \times \lambda(t) \times R_n$ , where  $k$  is a site-specific constant that scales  $R_n$ , calibrated against  $ET_{obs}$  and  $R_n$  was converted to mass units ( $\text{mm d}^{-1}$ ) by multiplying it by the latent heat of vaporization ( $\text{J kg}^{-1}$ ) as a function of air temperature, using the R package 'BIGLEAF' (Knauer *et al.*, 2018).

### Derivation of the cumulative water deficit

To evaluate how fET evolves in progressing drought conditions, we regressed it against the CWD. We derived the CWD as the cumulative difference in the actual evapotranspiration ( $ET_{obs}$ ) and precipitation ( $P$ ), considered over continuous dry periods, that is, periods where the difference  $P - ET_{obs}$  was negative. We defined a 'CWD event' as the period between the start and the end of the summation. The summation was stopped when the rain had compensated the water loss due to ET, that is, the cumulative sum across days was zero ( $\sum_{i=1}^{ndays} (P - ET) = 0$ ), where  $ndays$  refers to the number of days within a 'CWD event' (Fig. S6). We assumed that water stress was already mitigated when new precipitation was re-wetting the topsoil layers, even before the CWD was fully offset, that is, before the deficit reached a value of zero. For this reason, we removed data after rain had compensated the CWD to 90% of its maximum value within the same 'CWD event'.

To eliminate the noise caused by smaller CWD events and focus on extreme events, we only retained the single largest CWD event each year. For the CWD calculation of the fET plots, we used the observed latent heat flux and precipitation time series from FLUXNET2015 at the daily time scale. When employing  $fET_{GLDAS}$ , CWD was computed with precipitation and ET data from the GLDAS product for consistency.



**Fig. 1** Location of sites considered in this study, colored by their respective group of fractional reduction in evapotranspiration (fET group, see the [Site selection and binning](#) section). Blue dots: 'high fET' group. Yellow dots: 'medium fET' group. Red dots: 'low fET' group. Black crosses: sites that were excluded from the initial list of 135 sites considered in this study. Coastlines were downloaded using R package 'RNATURALEARTH' (Massicotte & South, 2023).

When calculating CWD, it was important to focus on high-quality observations and use a continuous time series of ET to avoid gaps. We therefore processed the data in a different way compared with the DNN models, as described in Section 4 of Methods S1.

### Site selection and binning

We performed our analysis for 135 sites out of the total of 166 of the FLUXNET Tier 1 dataset (Fig. 1), where soil moisture gave consistent results (as defined in the [Soil moisture data](#) section). The sites were further filtered according to the final number of days after data cleaning ( $> 300$  d) and to the performance of the DNN model. Mean  $PET_{NN}$  had to be greater than or equal to ET during 'dry days' and the  $R^2$  between modelled ET and  $ET_{obs}$  had to be  $> 0.5$ , retaining 58 sites. Nine sites were excluded upon visual inspection of the fET vs CWD relationship, which was not giving physically consistent results. The remaining 49 sites were used in this study and are listed in Table S1 and displayed in Fig. 1. We removed fET outliers, defined as any value that fell outside of the interval  $\overline{fET} \pm 2.5 \times \text{std}(fET)$ . To categorize the behavior of different sites, we calculated the median of fET in the CWD interval comprised between 125 and 175 mm for each site. We grouped all sites along this single dimension using a  $k$ -means algorithm, with predefined  $k=3$ . We conducted a sensitivity analysis with  $k=2$  and  $k=4$ . We retained the grouping with  $k=3$ , as it identified clearly the dominant fET distributions across sites. The resulting groups were high fET (8 sites), medium fET (22 sites) and low fET (11 sites), with each group showing a similar pattern in the decline of fET with increasing CWD. Sites that had a maximum CWD  $< 125$  mm were manually assigned to the 'high fET' group (8 sites), as their behavior was visually deemed to be consistent with other sites in the same

group (Fig. S7). The CWD interval centered at 150 mm was a trade-off between using the largest possible CWD, thus capturing the most divergent responses across sites, and choosing a CWD value attained and exceeded in the largest number of sites. The three fET groups, thus defined, were intended as a measure of the sensitivity of fET to increasing CWD, targeting the different fET vs CWD shapes observed at different sites.

## Results

### Reliability of the deep neural network

Across all sites and days,  $ET_{NN}$  achieved consistent results against  $ET_{obs}$  ( $R^2 = 0.78$ ; Fig. 2a). To evaluate the accuracy of  $PET_{NN}$ , we compared it against  $ET_{obs}$  during moist days only ( $R^2 = 0.77$ ; Fig. 2b). This method matched observations more closely compared with  $PET_{PT}$  ( $R^2 = 0.45$ ; Fig. 2c) or  $PET_{lm}$  ( $R^2 = 0.40$ ; Fig. 2d), both evaluated for moist days only. We thus retained  $PET_{NN}$  for further analyses.

To understand the timing and magnitude of water limitation on  $ET_{obs}$ , we evaluated its seasonality compared with  $ET_{NN}$  and  $PET_{NN}$  (Figs 3, S8). We chose two sample sites with contrasting behavior: DK-Sor, a humid deciduous broadleaf forest, and US-Ton, a dry woody savannah site. At DK-Sor,  $PET_{NN}$  and  $ET_{obs}$  almost perfectly overlap, suggesting that belowground moisture limitation has little effect on ET at this site, allowing it to be almost always at its potential rate, that is, energy-limited and without belowground moisture limitations (Fig. 3a, red and black lines). At US-Ton,  $PET_{NN}$  departs substantially from  $ET_{obs}$  during the dry season, indicating significant impacts of water stress on ET at this site (Fig. 3b, red and black lines). In both cases,  $ET_{NN}$  is consistent with  $ET_{obs}$  (black and blue lines) and the ET seasonality follows the seasonality of  $R_n$  (Fig. 3, dashed green line).

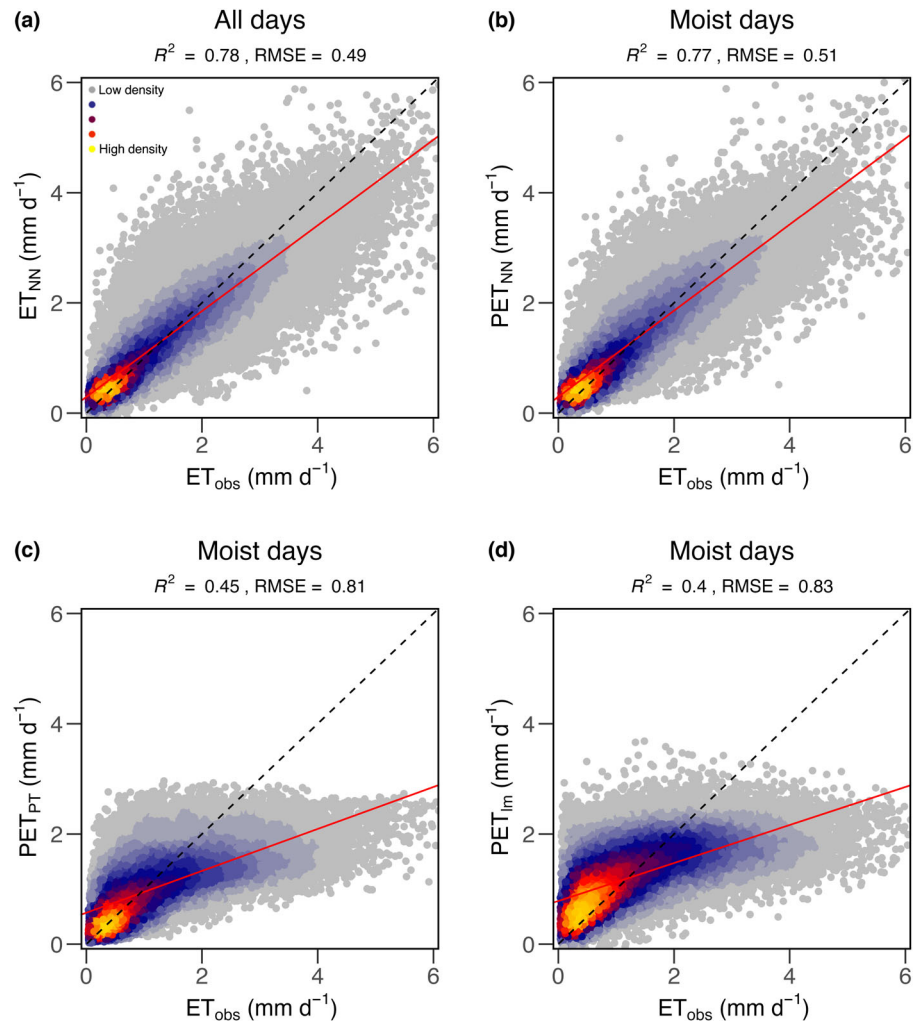


**Fig. 2** Performance of the deep-learning model at predicting evapotranspiration (ET).  $ET_{NN}$  and potential evapotranspiration ( $PET_{NN}$ ) are respectively ET and PET predicted with our deep-learning model.  $ET_{obs}$  corresponds to observational ET from FLUXNET2015. (a)  $ET_{NN}$  vs  $ET_{obs}$ , evaluated on all days. (b)  $PET_{NN}$  vs  $ET_{obs}$ , evaluated on moist days only. (c)  $PET_{PT}$  is from the SPLASH model, based on a Priestley–Taylor formulation of evapotranspiration, vs  $ET_{obs}$ . To align its magnitude with that of  $ET_{obs}$ ,  $PET_{PT}$  was multiplied by a scaling constant. This does not impact the  $R^2$  between the two variables. (d)  $PET_{lm}$  is based on a linear model (lm), defined as  $PET = k \times \lambda(t) \times R_n$ , where  $k$  is a site-specific constant that scales  $R_n$ , calibrated to  $ET_{obs}$  and  $R_n$  was converted to mass units ( $mm\ d^{-1}$ ) by multiplying it by the latent heat of vaporization ( $J\ kg^{-1}$ ). Red line: regression line between modelled and observed data. Dashed black line:  $y = x$  line. RMSE, root-mean-square error. R package ‘LSD’ was used to plot the point density (Schwalb *et al.*, 2020).

### Binning of fET vs CWD responses

When the density of fET is plotted against CWD across all sites, we observe a variety of responses (Fig. 4a). For CWD values up to  $c. 100$  mm, there is an accumulation of points centered at fET equal to  $c. 1$ . At higher CWD values, fET declines gradually. We can distinguish two other smaller clouds of points, one centered at fET equal to  $c. 0.4$  and another one at  $0.2$ . The response of fET vs CWD seems to be the most variable at CWD equal to  $c. 150$  mm (red dotted lines in Fig. 4a). To further investigate commonalities of the fET–CWD relationship across sites, we divided them into three groups based on the fET median in this interval (Fig. 4b; see the Derivation of the cumulative water deficit section). Sites were thus grouped into low, medium and high fET. Each group exhibits a different fET vs CWD behavior (Fig. 5).

### Patterns of fET vs CWD responses across sites

At ‘high fET’ sites, there is almost no effect of water stress on plants, as fET is almost always near one, in spite of substantial water deficits (Figs 5a, S7). By contrast, when predicted by a standard LSM, after a CWD threshold of  $c. 150$  mm,  $fET_{GLDAS}$  decreases linearly with progressing drought at these sites (Fig. 5b).

At ‘medium fET’ sites (Fig. 5c), the bulk of fET values is equal to one up to a CWD of  $c. 100$  mm. At a CWD  $> 100$  mm, fET slowly decreases with progressing CWD, reaching an fET of  $c. 0.5$  at a corresponding CWD of 250 mm. By contrast,  $fET_{GLDAS}$  displays several tails, which decrease linearly with progressing CWD, down to zero (Fig. 5d). The observed  $fET_{GLDAS}$  behavior reflects different responses at different sites (not shown). At ‘low fET’ sites, fET stays equal to one until a CWD of 50 mm. After that, fET values drop off abruptly with increasing CWD, followed by a relationship that largely levels-off, slowly approaching but never reaching fET = 0 (Fig. 5e). In the same fET group,  $fET_{GLDAS}$  decreases almost linearly with progressing drought, reaching values of  $c. 0$  (Fig. 5f). This drop in fET with CWD followed by a levelling-off is also seen for each of the individual sites in this group (Fig. 6). This confirms that the trend observed in Fig. 5e is not simply due to plotting several sites pooled together and adds further support to the site grouping used here. Across the three fET groups,  $fET_{GLDAS}$  reduces more quickly with increasing CWD than fET does, suggesting GLDAS overestimates water stress. Plotting EF vs CWD confirmed the results found when using fET (Fig. S9). Using transpiration from a published data set (Li *et al.*, 2019) as target variable instead of ET resulted in lower model performance, but did not change our main conclusions (Fig. S10).

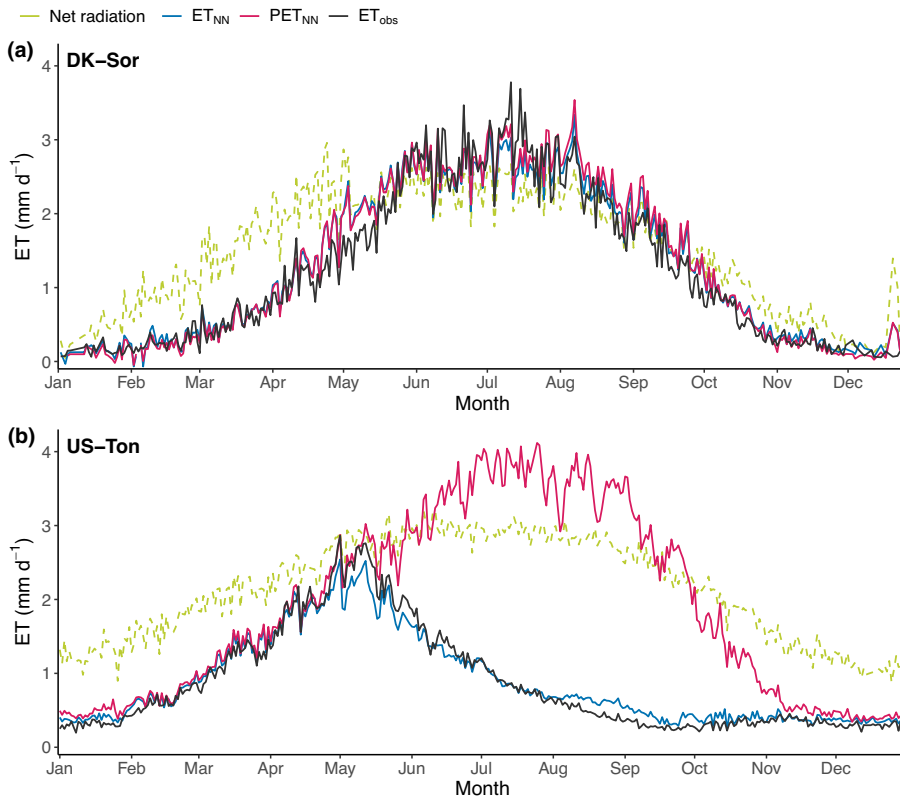


**Fig. 3** Seasonality of evapotranspiration (ET) and potential evapotranspiration (PET) at sample sites. (a) DK-Sor. (b) US-Ton.  $ET_{NN}$  and  $PET_{NN}$  are ET and PET predicted with our deep-learning model, respectively.  $ET_{obs}$  corresponds to observational ET from FLUXNET2015. Blue line:  $ET_{NN}$ . Red line:  $PET_{NN}$ . Black line:  $ET_{obs}$ . Dashed green line: net radiation converted to mass units ( $\text{mm d}^{-1}$ ). We derived the seasonality by calculating the mean across all years for every day of the year.

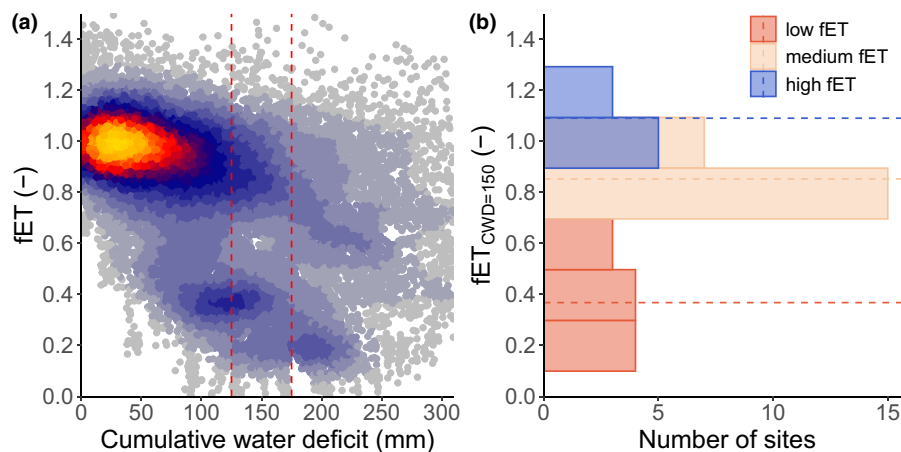


**Fig. 4** Partition of sites in three groups according to the median of the fractional reduction in evapotranspiration (fET) at a cumulative water deficit (CWD) equal to 150 mm. (a) fET for all sites plotted against the CWD. Dashed lines at  $CWD = 125$  mm and  $CWD = 175$  mm delimit the interval ( $fET_{150}$ ) in which the median of fET was calculated for each site to define the three fET groups ('low fET', 'medium fET' and 'high fET'). R package 'LSD' was used to plot the point density (Schwalb *et al.*, 2020). (b) Number of sites per each fET group: 'low fET' sites (red), 'medium fET' sites (green) and 'high fET' sites (blue). Dashed lines represent the average fET inside each group. The width of the bins was determined with the Freedman–Diaconis rule, which considers not only sample size but also the spread of each sample.

### Relationship to soil and climate variables

To gain insight into what factors drive the different fET behaviors, we investigated how soil and climate variables vary within site groups (Fig. 7). Soil texture did not vary significantly among fET groups (Fig. 7a). Sites in the 'high fET' group were usually found in humid climates (Fig. 7c). They consisted mostly of forests, and in particular evergreen needleleaf forest (ENF, 7 sites

out of 16, Fig. 7b). We found that sites with intermediate fET reductions were found in mesic regions (Fig. 7c). They were mostly characterized by forests (14 sites out of 22) and croplands (four sites, Fig. 7b). The 'low fET' sites were found in the driest climates (Fig. 7c). These sites were composed mostly of savannahs (five sites over 11) and grasslands (four sites over 11; Fig. 7b). The GTI and mean annual precipitation did not vary significantly across fET groups (Fig. 7d,e). This is consistent with



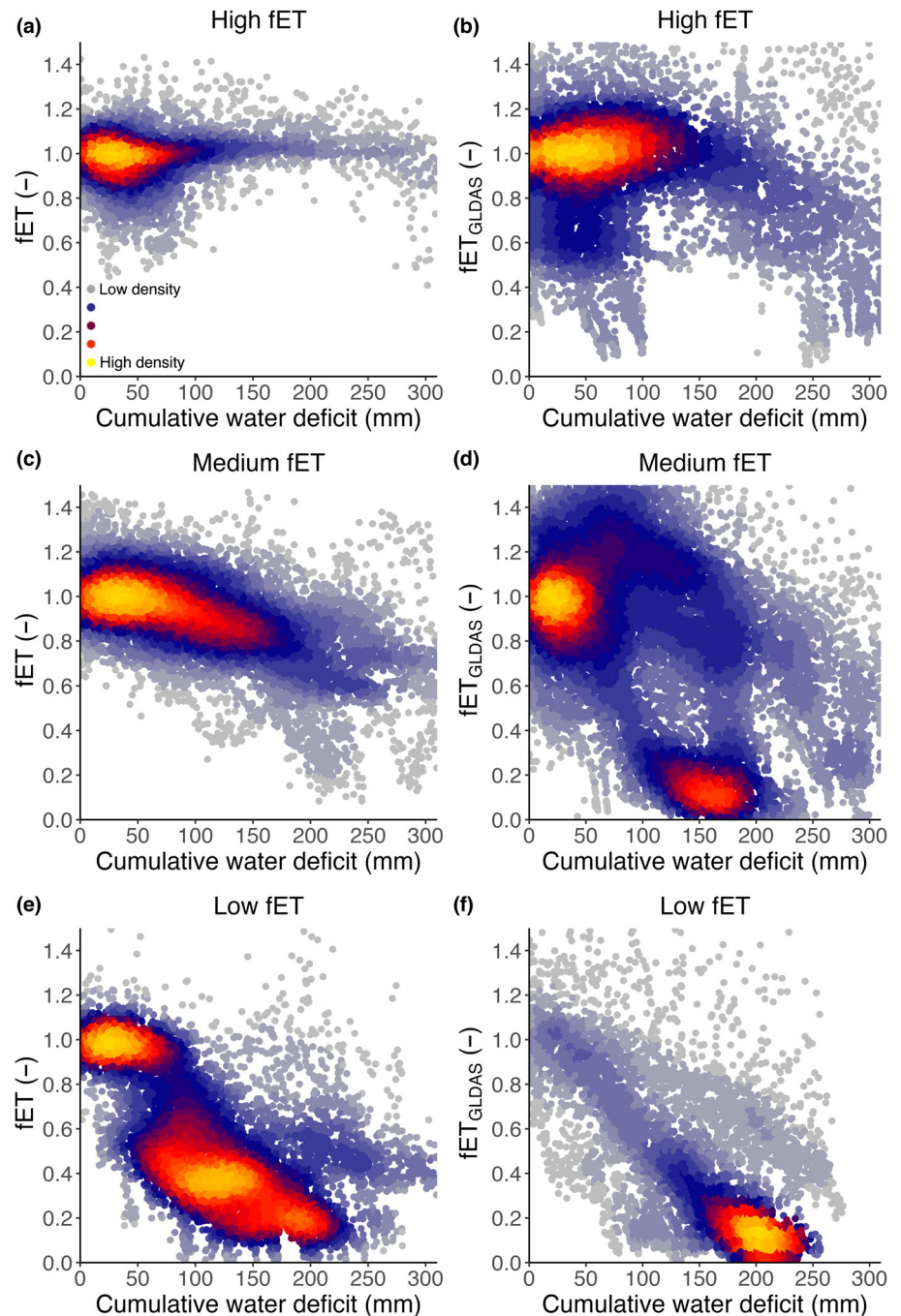


**Fig. 5** Evolution of the fractional reduction in evapotranspiration (fET) with the cumulative water deficit (CWD) for sites grouped according to their median fET. (a) 'High fET', fET predicted from our observations-driven model. (b) 'High fET', fET extracted from the GLDAS-NOAH data product ( $fET_{GLDAS}$ ). (c) 'Medium fET', fET predicted from our observations-driven model. (d) 'Medium fET', fET extracted from the GLDAS-NOAH data product. (e) 'Low fET', fET predicted from our observations-driven model. (f) 'Low fET', fET extracted from the GLDAS-NOAH data product.  $fET_{GLDAS}$  calculated as evapotranspiration (ET) divided by potential evapotranspiration (PET) from the GLDAS-NOAH data product, where PET was scaled by dividing it by its median in the lower CWD bin (CWD < 20 mm). When plotted against  $fET_{GLDAS}$ , CWD was calculated using GLDAS-NOAH data for consistency. R package 'LSD' was used to plot the point density (Schwalb *et al.*, 2020).

the fact that most flux towers are located in flat areas and valleys so that most sites cluster into similar topographic index values (Thompson *et al.*, 2011). By contrast, the MAT increases from high to low fET groups (Fig. 7f).

## Discussion

### Physical interpretation of CWD

Since the CWD is the integration of the observed water balance over time (see the [Site selection and binning](#) section), it constitutes a proxy for the depletion of plant available water. By

definition, the CWD is independent from assumptions regarding soil depth or total water storage capacity, thereby encompassing contributions from both soil and nonsoil water reservoirs, regardless of their depths (see the [Derivation of the cumulative water deficit](#) section). The connection between CWD and plant-accessible moisture reservoirs is implicit, as the presence of a deficit (resulting from plant water uptake and transpiration) necessitates the existence of a reservoir that stores the respective water.

Contrary to our expectations, we found that at most sites, vegetation activity is never completely shut off, even at high CWD values (Fig. 5a,c,e). This is also confirmed by EF, a model-independent indicator of ET stress, plotted as a function

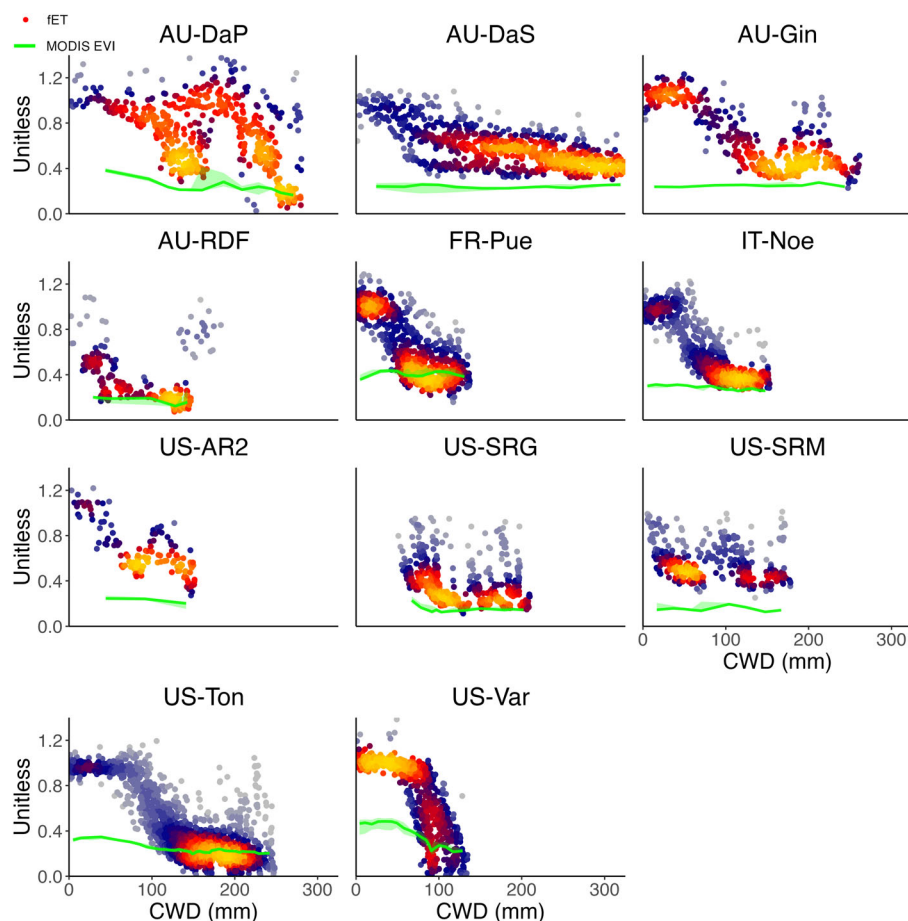


**Fig. 6** Evolution of the fractional reduction in evapotranspiration (fET) with the cumulative water deficit (CWD) for sites classified in the 'low fET' group. Colored dots: fET. Green line: MODIS Enhanced Vegetation Index (EVI). EVI was binned by CWD intervals of 50 points. Shading represents the lower and upper quartiles, and the solid line the median in every bin. R package 'LSD' was used to plot the point density (Schwalb *et al.*, 2020).

of CWD (Fig. S9). As CWD increases and fET decreases (Fig. 5a,c,e), the fET vs CWD pattern suggests that a mechanism must be put in place by plants to maintain a base ET level without further reductions in plant access to moisture, a pattern not reflected by a standard LSM (Fig. 5b,d,f).

### Drivers of the fET response to CWD

Under prolonged rain-free periods, plants have been shown to depend on water stored relatively deep below the surface (Milly, 1994; Hahm *et al.*, 2019; McCormick *et al.*, 2021) or to rely on very resistant xylems (Plaut *et al.*, 2012; Mackay *et al.*, 2015) to sustain function and growth. When water availability decreases in such a way that the root water potential decreases, one would also expect the xylem potential to decrease, and in turn the leaf water potential and the stomatal conductance, and thus ET. The relatively flat fET curve suggests that either (1) plants *resist* water stress, whereby conductance along the SPAC is relatively insensitive to the range of water potentials experienced by plants under the conditions investigated here, or (2) plants *limit* water stress, whereby plants access further, possibly deeper, water reservoirs and maintain relatively high water potentials along the SPAC while water is continuously consumed (thus continuously increasing the CWD). In the following paragraphs, we discuss the two abovementioned cases in more detail, including the specific conditions in which they could apply. Discerning with

a high level of confidence on a site-by-site basis between these two alternative explanations is beyond the scope of this study. Nevertheless, in the [Rooting strategies and plant conductance at arid sites](#) section we provide a more in-depth discussion from the literature focusing on field studies at some dry sites.

In case (1), the insensitivity would correspond to a specific range in the curve of the stomatal conductance as a function of leaf water potential, where the water potential varies without dramatically affecting the conductance (Wolf *et al.*, 2016). In this framework, plants would also have more resistant xylem, allowing them to pull water at lower water potentials. This could account for the sustained fET observed at some humid sites as well as the plateauing of the fET–CWD relationship observed at certain arid sites.

Our results indicate that plant sensitivity to CWD differs based on the moisture index of the site (Fig. 7c), which may reflect different adaptive plant strategies to water stress along a gradient of site mean aridity. The most resistant responses of ET to water deficits ('high fET' group) are observed – perhaps counterintuitively – in relatively moist climates. This seemingly contradicts existing knowledge of stomatal behavior and xylem vulnerability, which would typically suggest the opposite (Medlyn *et al.*, 2011; Lin *et al.*, 2015). However, in humid climates, mostly woody vegetation maintains activity during seasonal water deficits, possibly thanks to roots that access saturated layers, which are generally closer to the surface compared with arid regions (Fan *et al.*, 2017; Miguez-Macho & Fan, 2021). In

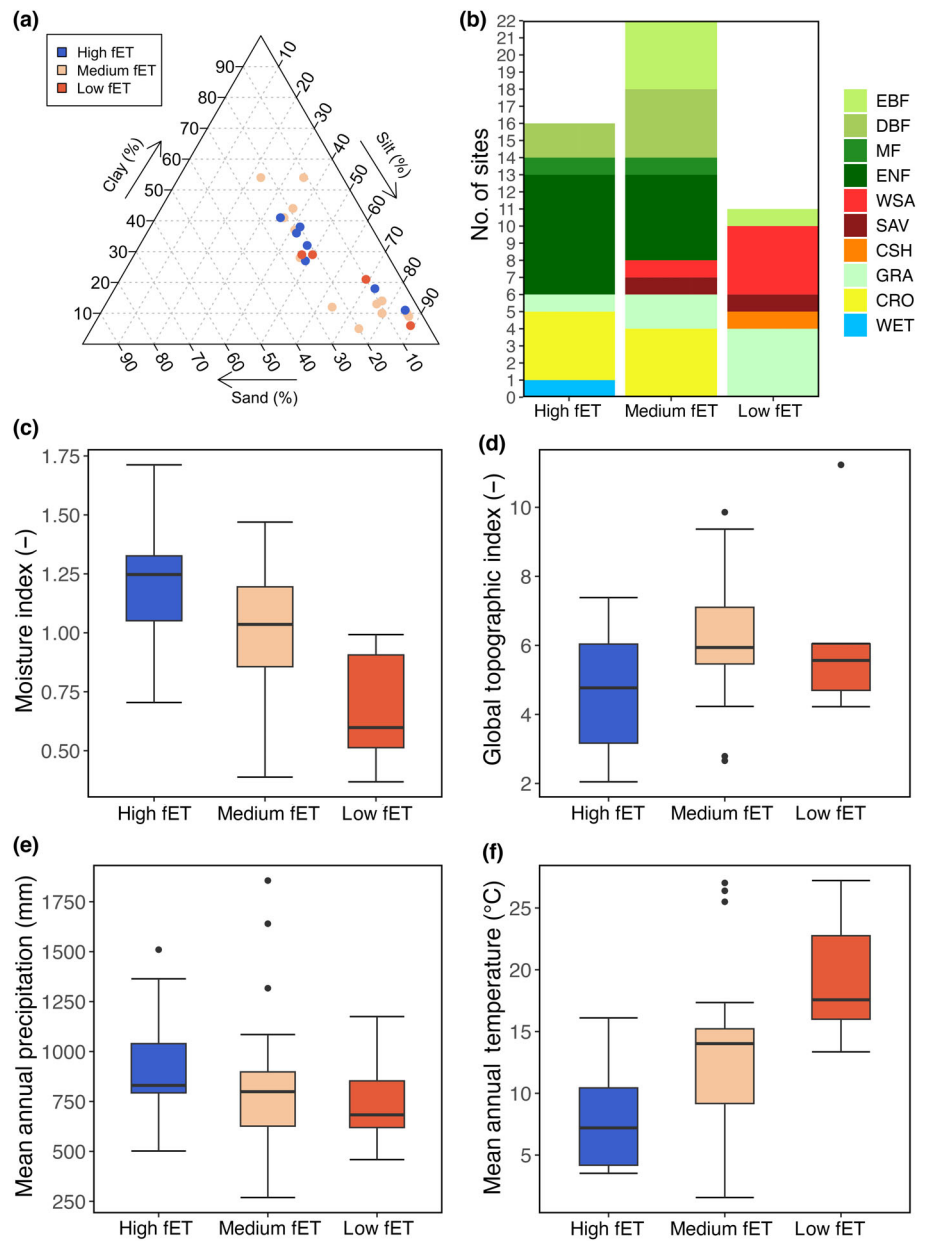


**Fig. 7** Analysis of soil and climate variables per group of fractional reduction in evapotranspiration (fET) group, see the [Site selection and binning](#) section). (a) Triangular plot of soil texture, colored by site, plotted with R package ‘PLOTRIX’ (Lemon, 2006). Note that some sites are overlapping. (b) IGBP vegetation classes (CRO, cropland; CSH, closed shrubland; DBF, deciduous broadleaf forest; EBF, evergreen broadleaf forest; ENF, evergreen needleleaf forest; GRA, grasslands; MF, mixed forest; SAV, savannah; WET, wetland; WSA, woody savannah). (c) Moisture index, defined as the ratio of annual precipitation (*P*) over potential evapotranspiration (PET), calculated for all available years on a site-by-site basis. Precipitation data was taken from the FLUXNET2015 dataset, whereas PET was calculated with the SPLASH model, based on a Priestley–Taylor formulation of evapotranspiration. (d) Global topographic index (GTI), defining the tendency of the soil to become saturated with water because of its topographic position. Higher GTI values are typical in valleys, whereas lower values are most common at ridgetops. (e) Mean annual precipitation (MAP). (f) Mean annual temperature (MAT). The bold black lines in the boxplots represent the median. The lower and upper hinges correspond to the first and third quartiles. Data beyond the hinges are plotted individually.

more arid environments, carbon uptake is limited and investments into structures for maintaining activity and access to water during dry spells (e.g. evergreen foliage and deep roots) are not competitively advantageous (Christiansen *et al.*, 1987; Stamp, 2003). Deep water tables and shallow water infiltration depths in arid sites (except along narrow riparian zones; Fan *et al.*, 2019) likely pose limitations to plant adaptation strategies for maintaining activity during dry seasons. Instead, plants have more resistant to xylem and follow drought-deciduous phenological strategies to reduce transpiration rates and water consumption (McDowell *et al.*, 2008). This is consistent with the xylem cavitation resistance found in arid plant communities (Jacobsen *et al.*, 2007). Nevertheless, the sustained evapotranspiration (fET) often observed at high water deficits (CWD) across different climates implies that water continues to be accessed and consumed without compromising transpiration efficiency. This

points to mechanisms that enable water stress avoidance rather than resistance.

Our findings generally align with the notion that forests (prevalent in ‘high fET’ sites) tend to have deeper roots that can access deeper water stores and therefore are more resilient to high CWD, which correspond to case 2) above (Fan *et al.*, 2017; Tumber-Dávila *et al.*, 2022). Instead, grasslands tend to have shallower roots (Tumber-Dávila *et al.*, 2022) and are thus more likely to experience water stress when the topsoil dries out. Therefore, forests tend to be less sensitive to drought than grasslands and can sustain vegetation activity over longer dry periods (Teuling *et al.*, 2010; Konings & Gentine, 2017; Martínez-Vilalta & García-Forner, 2017). However, we found several cropland and grassland sites within the ‘high fET’ group, suggesting that sustained water availability during dry periods is not limited to forests. This occurrence may be attributed to the interplay of

rooting depth and the depth of moisture stores, which can be relatively shallow in grassland and cropland areas (Fan *et al.*, 2019).

The different behavior observed in grasslands and forests may explain the drop in fET after an intermediate CWD threshold at some 'low fET' sites (Fig. 5e). In this group, the most common PFT is woody savannah (Fig. 7b), a tree–grass ecosystem characterized by a herbaceous understory (grassland) scattered with sufficiently spaced trees, so that the canopy is never continuous (Luo *et al.*, 2018; El-Madany *et al.*, 2020). After a certain CWD value (*c.* 50 mm), the herbaceous layer loses access to water and thus stops contributing to ecosystem ET. In turn, trees can rely on deep roots to access deeper water reservoirs. These strategies allow trees to keep transpiring even at higher CWD. This could explain why we observe an abrupt change in fET, followed by a levelling-off which never reaches zero (Fig. 5e). In this framework, the levelling-off corresponds to a period where activity of the understory ceases and trees are the primary contributors to the remaining ET.

### Rooting strategies and plant conductance at arid sites

Semi-arid regions are a key driver of the interannual variability of the terrestrial carbon cycle (Poulter *et al.*, 2014; Ahlström *et al.*, 2015). The diversity of seasonal reductions in ET found at arid and semi-arid sites suggest that a more accurate modelling of drought impacts in these areas could improve the prediction of the variability of the carbon cycle (Van der Molen *et al.*, 2011; Biederman *et al.*, 2017). This section presents some site-specific analyses from the literature that provide insight into our findings, focusing on dry sites with relevant field evidence.

US-Ton and US-Var, located in the lower foothills of the Sierra Nevada range in California, serve as an ideal case study due to their shared Mediterranean climate (Koeppen: Csa) and close proximity of 2.8 km (Baldocchi *et al.*, 2004). US-Var, an annual grassland, ceases activity (fET = 0) when CWD reaches *c.* 100 mm (Fig. 6), corresponding to the seasonal dry-down of grasses. US-Ton, an oak savanna woodland, continues transpiring even at CWD values exceeding 200 mm (Fig. 6). Field studies suggest that trees at US-Ton regulate their stomatal and hydraulic conductance to maintain transpiration at low water potentials, while also accessing deeper water reservoirs beyond the reach of grasses (< 0.6 m; Baldocchi *et al.*, 2004; Baldocchi & Xu, 2007). The availability of groundwater in the woodland site explains the interannual variation in ET with the grassland site, which lacks groundwater access (Baldocchi *et al.*, 2021).

A comparative analysis of Mediterranean oak woodlands at FR-Pue, IT-Cpz, IT-Ro2 and US-Ton reveals that down-regulation of photosynthesis and extensive root systems able to tap groundwater enable sustained transpiration during the dry season (Baldocchi *et al.*, 2010). Roots at FR-Pue extend to depths of 4.5 m (Allard *et al.*, 2008), while at IT-Cpz the shallow water table mitigates the effect of the dry season (Manes *et al.*, 1997). Our study categorizes FR-Pue and US-Ton as 'low fET' sites, and IT-Cpz and IT-Ro2 as 'medium fET' sites. In all four locations, a distinct levelling-off in the fET vs CWD relationship is

observed (Figs 6, S11), although the drop in fET is less pronounced in the 'medium fET' sites.

At AU-How, a North Australian eucalypt woody savannah classified as 'medium fET', the fET vs CWD curve levels off after an initial decline, maintaining *c.* 0.4 fET up to a CWD of 300 mm (Fig. S11). Groundwater availability sustains ET during drought in this region (O'Grady *et al.*, 1999). Finally, at AU-Cum, a native *Eucalyptus* woodland, trees access water stored in the soil at depths exceeding 4 m, enabling continued transpiration even under extremely dry conditions (Duursma *et al.*, 2011; Gimeno *et al.*, 2018). This is reflected in our findings, as AU-Cum is classified as a 'medium fET' site and sustains transpiration up to CWD values of 300 mm (Fig. S11).

In general, both groundwater and water stored deep in the unsaturated zone may be responsible for the observed fET vs CWD patterns at different sites. Further field studies could be devised to gain insight at other sites, using measurements that are linked to ET and can directly sample water in the soil–plant–atmosphere continuum (SPAC), that is, sap flow and leaf water potential measurements (Novick *et al.*, 2022). Water isotopes could also be employed to investigate the origin of water consumed by the plants at the site level (Brinkmann *et al.*, 2018).

### Possible explanations of the discrepancy between model and observations-driven estimates

The hypothesis that trees access deeper water reservoirs is consistent with recent findings, which highlight the often-neglected importance of deep water stores for root water uptake (Dawson *et al.*, 2020). These water reservoirs are often accessible to plants (McCormick *et al.*, 2021), but are essentially not represented by models, and are especially important during drought, after soil moisture is depleted (Rempe & Dietrich, 2018). This could explain why the lower tail of the fET vs CWD relationship in the 'low fET' group almost never reaches zero, even at very high CWD (i.e. under ongoing drought, Fig. 5e). The same behavior is not captured by the considered GLDAS model, which – like other land models – cannot quantify deep moisture (Fig. 5f).

Groundwater contributions to ET may explain the discrepancy between the considered GLDAS model data and the observation-driven estimates. Groundwater is generally not taken into account by global models (Hain *et al.*, 2015; Condon *et al.*, 2021), but it has been shown to have a pivotal effect on transpiration during drought (Mu *et al.*, 2021). The neglect of groundwater in many LSMs could explain why GLDAS-NOAH appears to overestimate water stress effects compared with our deep-learning estimates (Fig. 5b,d,f). This is consistent with a previous study finding that the quantification of plant access to groundwater in models can improve ET prediction (Thompson *et al.*, 2011).

We should highlight that the current comparison is only with one LSM. Comparisons with other LSMs would be necessary to confirm this hypothesis. Furthermore, while the observations-driven estimates used are strongly based on observations, they are also derived from an empirical model. A limitation of our deep-learning models is that they use EVI (vegetation greenness index)

as predictor, thus factoring out effects by reduced foliage area. When ET is essentially zero and the vegetation is brown (i.e. there are strong EVI reductions),  $PET_{NN}$  values may also be decreasing along with EVI. The decline in  $PET_{NN}$  would thus cancel at least a part of the decline in  $ET_{NN}$ , and we may have  $fET$  (defined as  $ET_{NN}/PET_{NN}$ ) values higher than expected. In these circumstances, we should be cautious when interpreting  $fET$  values (Figs 6, S7, S11). Nevertheless, situations with strong EVI reductions, matched with still high  $fET$  values, were only identified in sites US-Ne2 and DE-Geb ('medium  $fET$ ' group; Fig. S11) and US-Ne1 ('high  $fET$ ' group; Fig. S7).

GLDAS-NOAH uses vegetation tiling to represent sub-grid heterogeneity of vegetation types. NOAH assigns a rooting depth to each vegetation type (Rodell *et al.*, 2004; Beaudoin *et al.*, 2020) and does not account for heterogeneity in stomatal or xylem traits within the same vegetation type (Liu *et al.*, 2021). This could explain why GLDAS data does not capture some of the water stress responses highlighted by our approach, as the rooting depth has been shown to vary strongly even within the same species and climate (Fan *et al.*, 2017). The almost linear signal found in 'high  $fET$ ' sites when using GLDAS data (Fig. 5f) could also be linked to missing spatial heterogeneity in the model simulations. There is an intrinsic challenge in ET prediction related to the fact that soil moisture, and by extension below-ground water availability, varies in nature at scales in the order of 1–10 m, while models have grid cell sizes at scales as big as one to several hundred kilometers. The upscaling would naturally smooth out the stress response (Baker *et al.*, 2017) and produce an ecosystem response more linear than what it really is. In other words, large-scale averaging could lead to a less abrupt regulation of  $fET$  (Baker *et al.*, 2017). In general, models have less uncertainty than observations, which are by their nature more scattered. This could also explain the observed 'cleaner' relationships between  $fET_{GLDAS}$  and CWD.

Although the overestimation of water stress by LSMs is well-known in the literature, our findings underscore the lack of an accurate representation of water stored in the deep subsurface in models. More research could address the apparent model-observation bias in light of the role of belowground water availability.

## Conclusions

An observation-driven empirical approach was used to evaluate the effects of water stress on ET, separated from the contribution of other drivers, including radiation, VPD and vegetation greenness. We highlighted substantial differences in plant responses to water stress across vegetation types, mean site climate and soil texture. Most forests tend to show little sensitivity to water stress, whereas most savannahs, shrublands and grasslands sites show an abrupt drop in ET after an initial stress-free phase. In both cases and in contrast with a representative LSM, ET is almost never completely shut off, even during progressing drought conditions. Field studies confirmed that ET can be sustained during drought thanks to a combination of access to groundwater or deep soil moisture and down-regulation of stomatal closure with

progressive water deficits. The fact that most models do not account for sub-grid heterogeneity in plant available water and ignore moisture supplied by the saturated zone and weathered bedrock leads to a biased quantification of water stress effects on plants. Future research should address this bias by focusing on the role of deep unquantified water stores, the quantification of sub-grid heterogeneity, and the representation of rooting strategies and plant conductance across aridity gradients.

## Acknowledgements

The authors thank group members Koen Hufkens and Laura Marqués for providing feedback. We also thank the providers of the data sets used in this study, in particular NASA members R. Hualan, H. K. Beaudoin and M. Rodell for helpful comments. This project was supported by the generosity of Eric and Wendy Schmidt by recommendation of the Schmidt Futures program. FG and BDS were funded by the Swiss National Science Foundation grant no. PCEFP2\_181115. AGK was supported by National Science Foundation DEB-1942133 and by the NASA MAP program under award 80NSSC21K1523. PG was supported by the European Research Council grant SMILE: Understanding and modelling the Earth System with Machine Learning, by the NASA funding Remote Sensing Estimate of Evapotranspiration Partitioning to Transpiration and the NASA SMAP Understanding memory effects and climatic drivers of net primary productivity and respiration enabled by SMAP vegetation optical depth (with AGK). Open access funding provided by Eidgenössische Technische Hochschule Zurich.






## Competing interests

None declared.

## Author contributions

FG, BDS, PG and AGK designed the study and wrote the first version of the manuscript. FG, BDS, PG, AGK and SIS commented and revised the manuscript. FG performed the analysis and prepared the figures.

## ORCID

Pierre Gentine  <https://orcid.org/0000-0002-0845-8345>  
Francesco Giardina  <https://orcid.org/0000-0002-8359-809X>  
Alexandra G. Konings  <https://orcid.org/0000-0002-2810-1722>  
Sonia I. Seneviratne  <https://orcid.org/0000-0001-9528-2917>  
Benjamin D. Stocker  <https://orcid.org/0000-0003-2697-9096>

## Data availability

All intermediate data and computer codes that support this study are available from the Zenodo Digital Repository: <https://zenodo.org/badge/latestdoi/588230432> (Giardina, 2023). The

modelled fET output is also made available as a separate dataset: <https://doi.org/10.5281/zenodo.6885163>.

All original datasets used in this study are freely available from the following sources:

- Ecosystem fluxes and meteorological data: <https://fluxnet.org/data/fluxnet2015-dataset/>
- MODIS EVI (from MOD13Q1, 16 d, 250 m): <https://lpdaac.usgs.gov/products/mod13q1v006/>
- Precipitation, ET and PET estimates from the GLDAS\_NOAH025\_3H\_2.1 product: [https://disc.gsfc.nasa.gov/datasets/GLDAS\\_NOAH025\\_3H\\_2.1/summary](https://disc.gsfc.nasa.gov/datasets/GLDAS_NOAH025_3H_2.1/summary)
- Soil texture distribution data: <https://daac.ornl.gov/SOILS/guides/HWSD.html>
- Mean annual temperature (MAT) and mean annual precipitation (MAP): <https://www.worldclim.org/data/worldclim21.html>
- Global topographic index (GTI): <https://data-search.nerc.ac.uk/geonetwork/srv/api/records/6b0c4358-2bf3-4924-aa8f-793d468b92be>

## References

- Ahlström A, Raupach MR, Schurgers G, Smith B, Arneth A, Jung M, Reichstein M, Canadell JG, Friedlingstein P, Jain AK *et al.* 2015. The dominant role of semi-arid ecosystems in the trend and variability of the land CO<sub>2</sub> sink. *Science* 348: 895–899.
- Allard V, Ourcival JM, Rambal S, Joffre R, Rocheteau A. 2008. Seasonal and annual variation of carbon exchange in an evergreen Mediterranean forest in southern France. *Global Change Biology* 14: 714–725.
- Baker IT, Sellers PJ, Denning AS, Medina I, Kraus P, Haynes KD, Biraud SC. 2017. Closing the scale gap between land surface parameterizations and GCMs with a new scheme, SiB3-Bins. *Journal of Advances in Modeling Earth Systems* 9: 691–711.
- Baldocchi DD, Ma S, Rambal S, Misson L, Ourcival J-M, Limousin J-M, Pereira J, Papale D. 2010. On the differential advantages of evergreenness and deciduousness in Mediterranean oak woodlands: a flux perspective. *Ecological Applications* 20: 1583–1597.
- Baldocchi DD, Ma S, Verfaillie J. 2021. On the inter- and intra-annual variability of ecosystem evapotranspiration and water use efficiency of an oak savanna and annual grassland subjected to booms and busts in rainfall. *Global Change Biology* 27: 359–375.
- Baldocchi DD, Xu L. 2007. What limits evaporation from Mediterranean oak woodlands – the supply of moisture in the soil, physiological control by plants or the demand by the atmosphere? *Advances in Water Resources* 30: 2113–2122.
- Baldocchi DD, Xu L, Kiang N. 2004. How plant functional-type, weather, seasonal drought, and soil physical properties alter water and energy fluxes of an oak-grass savanna and an annual grassland. *Agricultural and Forest Meteorology* 123: 13–39.
- Beaudoin H, Rodell M, NASA/GSFC/HSL. 2020. *GLDAS Noah land surface model L4 3 hourly 0.25 × 0.25 degree v.2.1*. Greenbelt, MD, USA: Goddard Earth Sciences Data and Information Services Center (GES DISC).
- Beer C, Reichstein M, Tomelleri E, Ciais P, Jung M, Carvalhais N, Rödenbeck C, Arain MA, Baldocchi D, Bonan GB *et al.* 2010. Terrestrial gross carbon dioxide uptake: global distribution and covariation with climate. *Science* 329: 834–839.
- Biederman JA, Scott RL, Bell TW, Bowling DR, Dore S, Garatuza-Payan J, Kolb TE, Krishnan P, Krofcheck DJ, Litvak ME *et al.* 2017. CO<sub>2</sub> exchange and evapotranspiration across dryland ecosystems of southwestern North America. *Global Change Biology* 23: 4204–4221.
- Brinkmann N, Seeger S, Weiler M, Buchmann N, Eugster W, Kahmen A. 2018. Employing stable isotopes to determine the residence times of soil water and the temporal origin of water taken up by *Fagus sylvatica* and *Picea abies* in a temperate forest. *New Phytologist* 219: 1300–1313.
- Christiansen E, Waring RH, Berryman AA. 1987. Resistance of conifers to bark beetle attack: searching for general relationships. *Forest Ecology and Management* 22: 89–106.
- Condon LE, Kollet S, Bierkens MFP, Fogg GE, Maxwell RM, Hill MC, Fransen HJH, Verhoef A, Van Loon AF, Sulis M *et al.* 2021. Global groundwater modeling and monitoring: opportunities and challenges. *Water Resources Research* 57: e2020WR029500.
- Dahlin KM, Fisher RA, Lawrence PJ. 2015. Environmental drivers of drought deciduous phenology in the Community Land Model. *Biogeosciences* 12: 5061–5074.
- Davis TW, Prentice IC, Stocker BD, Thomas RT, Whitley RJ, Wang H, Evans BJ, Gallego-Sala AV, Sykes MT, Cramer W. 2017. Simple process-led algorithms for simulating habitats (SPLASH v.1.0): Robust indices of radiation, evapotranspiration and plant-available moisture. *Geoscientific Model Development* 10: 689–708.
- Dawson TE, Hahm WJ, Crutchfield-Peters K. 2020. Digging deeper: what the critical zone perspective adds to the study of plant ecophysiology. *New Phytologist* 226: 666–671.
- Denissen JMC, Teuling AJ, Pitman AJ, Koirala S, Migliavacca M, Li W, Reichstein M, Winkler AJ, Zhan C, Orth R. 2022. Widespread shift from ecosystem energy to water limitation with climate change. *Nature Climate Change* 12: 677–684.
- Dralle DN, Jesse Hahm W, Rempe DM, Karst N, Anderegg LDL, Thompson SE, Dawson TE, Dietrich WE. 2020. Plants as sensors: vegetation response to rainfall predicts root-zone water storage capacity in Mediterranean-type climates. *Environmental Research Letters* 15: 104074.
- Drewniak BA. 2019. Simulating dynamic roots in the energy exascale earth system land model. *Journal of Advances in Modeling Earth Systems* 11: 338–359.
- Duursma RA, Barton CVM, Eamus D, Medlyn BE, Ellsworth DS, Forster MA, Tissue DT, Linder S, McMurtrie RE. 2011. Rooting depth explains (CO<sub>2</sub>) × drought interaction in *Eucalyptus saligna*. *Tree Physiology* 31: 922–931.
- Ek MB, Mitchell KE, Lin Y, Rogers E, Grunmann P, Koren V, Gayno G, Tarpley JD. 2003. Implementation of Noah land surface model advances in the National Centers for Environmental Prediction operational mesoscale Eta model. *Journal of Geophysical Research: Atmospheres* 108: 2002JD003296.
- El-Madany TS, Carrara A, Martín MP, Moreno G, Kolle O, Pacheco-Labrador J, Weber U, Wutzler T, Reichstein M, Migliavacca M. 2020. Drought and heatwave impacts on semi-arid ecosystems' carbon fluxes along a precipitation gradient: drought and heatwave impacts. *Philosophical Transactions of the Royal Society of London. Series B: Biological Sciences* 375: 20190519.
- Fan Y, Clark M, Lawrence DM, Swenson S, Band LE, Brantley SL, Brooks PD, Dietrich WE, Flores A, Grant G *et al.* 2019. Hillslope hydrology in global change research and earth system modeling. *Water Resources Research* 55: 1737–1772.
- Fan Y, Li H, Miguez-Macho G. 2013. Global patterns of groundwater table depth. *Science* 339: 940–943.
- Fan Y, Miguez-Macho G, Jobbágy EG, Jackson RB, Otero-Casal C. 2017. Hydrologic regulation of plant rooting depth. *Proceedings of the National Academy of Sciences, USA* 114: 10572–10577.
- Fan Y, Miguez-Macho G, Weaver CP, Walko R, Robock A. 2007. Incorporating water table dynamics in climate modeling: 1. Water table observations and equilibrium water table simulations. *Journal of Geophysical Research: Atmospheres* 112: D10125.
- Fick SE, Hijmans RJ. 2017. WorldClim 2: new 1-km spatial resolution climate surfaces for global land areas. *International Journal of Climatology* 37: 4302–4315.
- Gao H, Hrachowitz M, Schymanski SJ, Fenicia F, Sriwongsitanon N, Savenijie HHG. 2014. Climate controls how ecosystems size the root zone storage capacity at catchment scale. *Geophysical Research Letters* 41: 7916–7923.
- Giardina F. 2023. fgiardin/fET: accepted for publication (v2.0). *Zenodo*. doi: 10.5281/zenodo.8186408.
- Giardina F, Konings AG, Kennedy D, Alemohammad SH, Oliveira RS, Uriarte M, Gentile P. 2018. Tall Amazonian forests are less sensitive to precipitation variability. *Nature Geoscience* 11: 405–409.
- Gimeno TE, McVicar TR, O'Grady AP, Tissue DT, Ellsworth DS. 2018. Elevated CO<sub>2</sub> did not affect the hydrological balance of a mature native *Eucalyptus* woodland. *Global Change Biology* 24: 3010–3024.

- Green JK, Konings AG, Alemohammad SH, Berry J, Entekhabi D, Kolassa J, Lee J-E, Gentine P. 2017. Regionally strong feedbacks between the atmosphere and terrestrial biosphere. *Nature Geoscience* 10: 410–414.
- Hahm WJ, Dralle DN, Rempe DM, Bryk AB, Thompson SE, Dawson TE, Dietrich WE. 2019. Low subsurface water storage capacity relative to annual rainfall decouples Mediterranean plant productivity and water use from rainfall variability. *Geophysical Research Letters* 46: 6544–6553.
- Hain CR, Crow WT, Anderson MC, Tugrul Yilmaz M. 2015. Diagnosing neglected soil moisture source-sink processes via a thermal infrared-based two-source energy balance model. *Journal of Hydrometeorology* 16: 1070–1086.
- Jacobsen AL, Pratt RB, Davis SD, Ewers FW. 2007. Cavitation resistance and seasonal hydraulics differ among three arid Californian plant communities. *Plant, Cell & Environment* 30: 1599–1609.
- Kennedy D, Swenson S, Oleson KW, Lawrence DM, Fisher R, Lola da Costa AC, Gentine P. 2019. Implementing plant hydraulics in the community land model, v.5. *Journal of Advances in Modeling Earth Systems* 11: 485–513.
- Knauer J, El-Madany TS, Zaehle S, Migliavacca M. 2018. BIGLEAF – an R package for the calculation of physical and physiological ecosystem properties from eddy covariance data. *PLoS ONE* 13: 1–26.
- Konings AG, Gentine P. 2017. Global variations in ecosystem-scale isohydricity. *Global Change Biology* 23: 891–905.
- Lemon J. 2006. PLOTrix: a package in the red light district of R. *R-News* 6: 8–12.
- Li X, Gentine P, Lin C, Zhou S, Sun Z, Zheng Y, Liu J, Zheng C. 2019. A simple and objective method to partition evapotranspiration into transpiration and evaporation at eddy-covariance sites. *Agricultural and Forest Meteorology* 265: 171–182.
- Liang X, Lettenmaier DP, Wood EF, Burges SJ. 1994. A simple hydrologically based model of land surface water and energy fluxes for general circulation models. *Journal of Geophysical Research* 99: 14415.
- Lin YS, Medlyn BE, Duursma RA, Prentice IC, Wang H, Baig S, Eamus D, De Dios VR, Mitchell P, Ellsworth DS *et al.* 2015. Optimal stomatal behaviour around the world. *Nature Climate Change* 5: 459–464.
- Liu L, Gudmundsson L, Hauser M, Qin D, Li S, Seneviratne SI. 2020. Soil moisture dominates dryness stress on ecosystem production globally. *Nature Communications* 11: 1–9.
- Liu Y, Holtzman NM, Konings AG. 2021. Global ecosystem-scale plant hydraulic traits retrieved using model-data fusion. *Hydrology and Earth System Sciences* 25: 2399–2417.
- Liu Y, Kumar M, Katul GG, Feng X, Konings AG. 2020. Plant hydraulics accentuates the effect of atmospheric moisture stress on transpiration. *Nature Climate Change* 10: 691–695.
- Luo Y, El-Madany TS, Filippa G, Ma X, Ahrens B, Carrara A, Gonzalez-Cascon R, Cremonese E, Galvagno M, Hammer TW *et al.* 2018. Using near-infrared-enabled digital repeat photography to track structural and physiological phenology in Mediterranean tree-grass ecosystems. *Remote Sensing* 10: 1293.
- Mackay DS, Roberts DE, Ewers BE, Sperry JS, McDowell NG, Pockman WT. 2015. Interdependence of chronic hydraulic dysfunction and canopy processes can improve integrated models of tree response to drought. *Water Resources Research* 51: 6156–6176.
- Maes WH, Gentine P, Verhoest NEC, Miralles DG. 2019. Potential evaporation at eddy-covariance sites across the globe. *Hydrology and Earth System Sciences* 23: 925–948.
- Manes F, Grignetti A, Tinelli A, Lenz R, Ciccioli P. 1997. General features of the Castelporziano test site. *Atmospheric Environment* 31: 19–25.
- Marthews TR, Dadson SJ, Lehner B, Abele S, Gedney N. 2015a. High-resolution global topographic index values for use in large-scale hydrological modelling. *Hydrology and Earth System Sciences* 19: 91–104.
- Marthews TR, Dadson SJ, Lehner B, Abele S, Gedney N. 2015b. *High-resolution global topographic index values*. NERC Environmental Information Data Centre (Dataset).
- Martínez-Vilalta J, García-Fornier N. 2017. Water potential regulation, stomatal behaviour and hydraulic transport under drought: deconstructing the iso/anisohydric concept. *Plant, Cell & Environment* 40: 962–976.
- Massicotte P, South A. 2023. RNATURALEARTH: world map data from natural earth (0.3.2). [WWW document] URL <https://CRAN.R-project.org/package=rnaturalearth> [accessed 2 April 2023].
- McCormick EL, Dralle DN, Hahm WJ, Tune AK, Schmidt LM, Chadwick KD, Rempe DM. 2021. Widespread woody plant use of water stored in bedrock. *Nature* 597: 225–229.
- McDowell N, Pockman WT, Allen CD, Breshears DD, Cobb N, Kolb T, Plaut J, Sperry J, West A, Williams DG *et al.* 2008. Mechanisms of plant survival and mortality during drought: why do some plants survive while others succumb to drought? *New Phytologist* 178: 719–739.
- Medlyn BE, Duursma RA, Eamus D, Ellsworth DS, Prentice IC, Barton CVM, Crous KY, De Angelis P, Freeman M, Wingate L. 2011. Reconciling the optimal and empirical approaches to modelling stomatal conductance. *Global Change Biology* 17: 2134–2144.
- Meinzer FC, Johnson DM, Lachenbruch B, McCulloh KA, Woodruff DR. 2009. Xylem hydraulic safety margins in woody plants: coordination of stomatal control of xylem tension with hydraulic capacitance. *Functional Ecology* 23: 922–930.
- Miguez-Macho G, Fan Y. 2021. Spatiotemporal origin of soil water taken up by vegetation. *Nature* 598: 624–628.
- Miguez-Macho G, Fan Y, Weaver CP, Walko R, Robock A. 2007. Incorporating water table dynamics in climate modeling: 2. Formulation, validation, and soil moisture simulation. *Journal of Geophysical Research: Atmospheres* 112: 2006JD008112.
- Milly PCD. 1994. Climate, soil water storage, and the average annual water balance. *Water Resources Research* 30: 2143–2156.
- Miralles DG, Gentine P, Seneviratne SI, Teuling AJ. 2019. Land-atmospheric feedbacks during droughts and heatwaves: state of the science and current challenges. *Annals of the New York Academy of Sciences* 1436: 19–35.
- Mu M, De Kauwe MG, Ukkola AM, Pitman AJ, Guo W, Hobeichi S, Briggs PR. 2021. Exploring how groundwater buffers the influence of heatwaves on vegetation function during multi-year droughts. *Earth System Dynamics* 12: 919–938.
- Novick KA, Ficklin DL, Baldocchi D, Davis KJ, Ghezzehei TA, Konings AG, MacBean N, Raouf N, Scott RL, Shi Y *et al.* 2022. Confronting the water potential information gap. *Nature Geoscience* 15: 158–164.
- Novick KA, Ficklin DL, Stoy PC, Williams CA, Bohrer G, Oishi AC, Papuga SA, Blanken PD, Noormets A, Sulman BN *et al.* 2016. The increasing importance of atmospheric demand for ecosystem water and carbon fluxes. *Nature Climate Change* 6: 1023–1027.
- O'Grady AP, Eamus D, Hutley LB. 1999. Transpiration increases during the dry season: patterns of tree water use in eucalypt open-forests of northern Australia. *Tree Physiology* 19: 591–597.
- Orth R, Koster RD, Seneviratne SI. 2013. Inferring soil moisture memory from streamflow observations using a simple water balance model. *Journal of Hydrometeorology* 14: 1773–1790.
- Pastorello G, Trotta C, Canfora E, Chu H, Christianson D, Cheah Y-W, Poindexter C, Chen J, Elbashandy A, Humphrey M *et al.* 2020. The FLUXNET2015 dataset and the ONEFlux processing pipeline for eddy covariance data. *Scientific Data* 7: 225.
- Plaut JA, Yezzer EA, Hill J, Pangle R, Sperry JS, Pockman WT, McDowell NG. 2012. Hydraulic limits preceding mortality in a piñon-juniper woodland under experimental drought. *Plant, Cell & Environment* 35: 1601–1617.
- Poulter B, Frank D, Ciais P, Myneni RB, Andela N, Bi J, Broquet G, Canadell JG, Chevallier F, Liu YY *et al.* 2014. Contribution of semi-arid ecosystems to interannual variability of the global carbon cycle. *Nature* 509: 600–603.
- Prentice IC, Liang X, Medlyn BE, Wang YP. 2015. Reliable, robust and realistic: the three R's of next-generation land-surface modelling. *Atmospheric Chemistry and Physics* 15: 5987–6005.
- Qiu J, Crow WT, Nearing GS. 2016. The impact of vertical measurement depth on the information content of soil moisture for latent heat flux estimation. *Journal of Hydrometeorology* 17: 2419–2430.
- R Core Team. 2023. *R: a language and environment for statistical computing*. Vienna, Austria: R Foundation for Statistical Computing.
- Rempe DM, Dietrich WE. 2018. Direct observations of rock moisture, a hidden component of the hydrologic cycle. *Proceedings of the National Academy of Sciences, USA* 115: 2664–2669.
- Rodell M, Houser PR, Jambor U, Gottschalk J, Mitchell K, Meng CJ, Arsenault K, Cosgrove B, Radakovich J, Bosilovich M *et al.* 2004. The global land data assimilation system. *Bulletin of the American Meteorological Society* 85: 381–394.

- Ruddell BL, Kumar P. 2009. Ecohydrologic process networks: 1. Identification. *Water Resources Research* 45, W03419.
- Salvucci GD, Entekhabi D. 1994. Equivalent steady soil moisture profile and the time compression approximation in water balance modeling. *Water Resources Research* 30: 2737–2749.
- Schlemmer L, Schär C, Lüthi D, Strebel L. 2018. A groundwater and runoff formulation for weather and climate models. *Journal of Advances in Modeling Earth Systems* 10: 1809–1832.
- Schwab B, Tresch A, Torkler P, Duemcke S, Demel C, Ripley B, Venables B. 2020. *LSD: lots of superior depictions* (4.1-0). [WWW document] URL <https://CRAN.R-project.org/package=LSD> [accessed 15 October 2022].
- Schwalm CR, Williams CA, Schaefer K, Arneth A, Bonal D, Buchmann N, Chen J, Law B, Lindroth A, Luysaert S *et al.* 2010. Assimilation exceeds respiration sensitivity to drought: a FLUXNET synthesis. *Global Change Biology* 16: 657–670.
- Seneviratne SI, Corti T, Davin EL, Hirschi M, Jaeger EB, Lehner I, Orlowsky B, Teuling AJ. 2010. Investigating soil moisture–climate interactions in a changing climate: a review. *Earth-Science Reviews* 99: 125–161.
- Seneviratne SI, Lüthi D, Litschi M, Schär C. 2006. Land–atmosphere coupling and climate change in Europe. *Nature* 443: 205–209.
- Seneviratne SI, Zhang X, Adnan M, Badi W, Dereczynski C, Di Luca A, Ghosh S, Iskandar I, Kossin J, Lewis S *et al.* 2021. Weather and climate extreme events in a changing climate. *Climate Change 2021: The Physical Science Basis. Contribution of Working Group I to the Sixth Assessment Report of the Intergovernmental Panel on Climate Change*, Cambridge, in press.
- Stamp N. 2003. Out of the quagmire of plant defense hypotheses. *The Quarterly Review of Biology* 78: 23–55.
- Stocker BD, Tumber-Dávila SJ, Konings AG, Anderson MC, Hain C, Jackson RB. 2023. Global patterns of water storage in the rooting zones of vegetation. *Nature Geoscience* 16: 250–256.
- Stocker BD, Zscheischler J, Keenan TF, Prentice IC, Peñuelas J, Seneviratne SI. 2018. Quantifying soil moisture impacts on light use efficiency across biomes. *New Phytologist* 218: 1430–1449.
- Stocker BD, Zscheischler J, Keenan TF, Prentice IC, Seneviratne SI, Peñuelas J. 2019. Drought impacts on terrestrial primary production underestimated by satellite monitoring. *Nature Geoscience* 12: 264–270.
- Sulman BN, Roman DT, Yi K, Wang L, Phillips RP, Novick KA. 2016. High atmospheric demand for water can limit forest carbon uptake and transpiration as severely as dry soil. *Geophysical Research Letters* 43: 9686–9695.
- Swenson SC, Clark M, Fan Y, Lawrence DM, Perket J. 2019. Representing intrahillslope lateral subsurface flow in the community land model. *Journal of Advances in Modeling Earth Systems* 11: 4044–4065.
- Teuling AJ, Seneviratne SI, Stöckli R, Reichstein M, Moors E, Ciais P, Luysaert S, Van Den Hurk B, Ammann C, Bernhofer C *et al.* 2010. Contrasting response of European forest and grassland energy exchange to heatwaves. *Nature Geoscience* 3: 722–727.
- Teuling AJ, Seneviratne SI, Williams C, Troch PA. 2006. Observed timescales of evapotranspiration response to soil moisture. *Geophysical Research Letters* 33: 4.
- Thompson SE, Harman CJ, Konings AG, Sivapalan M, Neal A, Troch PA. 2011. Comparative hydrology across AmeriFlux sites: the variable roles of climate, vegetation, and groundwater. *Water Resources Research* 47: 1–17.
- Tuck SL, Phillips HRP, Hintzen RE, Hudson JPWS, Purvis A, Hudson NL. 2014. MODISTools – downloading and processing MODIS remotely sensed data in R. *Ecology and Evolution* 4: 4658–4668.
- Tumber-Dávila SJ, Schenk HJ, Du E, Jackson RB. 2022. Plant sizes and shapes above and belowground and their interactions with climate. *New Phytologist* 235: 1032–1056.
- Van der Molen MK, Dolman AJ, Ciais P, Eglin T, Gobron N, Law BE, Meir P, Peters W, Phillips OL, Reichstein M *et al.* 2011. Drought and ecosystem carbon cycling. *Agricultural and Forest Meteorology* 151: 765–773.
- Wickham H, Averick M, Bryan J, Chang W, McGowan L, François R, Grolemund G, Hayes A, Henry L, Hester J *et al.* 2019. Welcome to the tidyverse. *Journal of Open Source Software* 4: 1686.
- Wieder WR, Boehnert J, Bonan GB, Langseth M. 2014. *Regridded harmonized world soil database v.1.2*. Oak Ridge, TN, USA: ORNL DAAC.
- Wolf A, Anderegg WRL, Pacala SW. 2016. Optimal stomatal behavior with competition for water and risk of hydraulic impairment. *Proceedings of the National Academy of Sciences, USA* 113: E7222–E7230.
- Zhan S, Song C, Wang J, Sheng Y, Quan J. 2019. A global assessment of terrestrial evapotranspiration increase due to surface water area change. *Earth's Future* 7: 266–282.
- Zhang K, Kimball JS, Running SW. 2016. A review of remote sensing based actual evapotranspiration estimation. *Wiley Interdisciplinary Reviews: Water* 3: 834–853.
- Zhang Q, Manzoni S, Katul G, Porporato A, Yang D. 2014. The hysteretic evapotranspiration – vapor pressure deficit relation. *Journal of Geophysical Research Biogeosciences* 119: 125–140.
- Zhou S, Zhang Y, Williams AP, Gentile P. 2019. Projected increases in intensity, frequency, and terrestrial carbon costs of compound drought and aridity events. *Science Advances* 5: 1–9.

## Supporting Information

Additional Supporting Information may be found online in the Supporting Information section at the end of the article.

**Fig. S1** Evolution of the fractional reduction in evapotranspiration with the cumulative water deficit using observational vs modelled soil moisture data at US-Ton, US-Var, IT-CA3 and US-MMS.

**Fig. S2** Performance of the deep-learning model at predicting evapotranspiration and potential evapotranspiration, using the four predictors retained in the study vs a set of seven predictors.

**Fig. S3** Range and distribution of enhanced vegetation index for ‘moist’ and ‘dry’ days.

**Fig. S4** Seasonality of predicted and observed evapotranspiration, fractional reduction in evapotranspiration and enhanced vegetation index at US-Ton and US-SRG.

**Fig. S5** Performance of the deep-learning model at predicting evapotranspiration across sites.

**Fig. S6** Cumulative water deficit time series at sample site US-Ton, using FLUXNET2015 and GLDAS-NOAH data.

**Fig. S7** Fractional reduction in evapotranspiration (fET) vs cumulative water deficit for sites grouped according to their median fET. ‘High fET’ group.

**Fig. S8** Seasonality of predicted and observed evapotranspiration at two sample dry sites.

**Fig. S9** Evaporative fraction vs cumulative water deficit for sites grouped according to their median fractional reduction in evapotranspiration.

**Fig. S10** Evolution of the fractional reduction in evapotranspiration vs transpiration with the cumulative water deficit and performance of the deep-learning model at predicting evapotranspiration vs transpiration.



**Fig. S11** Fractional reduction in evapotranspiration (fET) vs cumulative water deficit for sites grouped according to their median fET. ‘Medium fET’ group.

**Methods S1** Extended description of data processing, deep-learning models and GLDAS product.

**Table S1** FLUXNET Tier 1 sites included in the analysis.

Please note: Wiley is not responsible for the content or functionality of any Supporting Information supplied by the authors. Any queries (other than missing material) should be directed to the *New Phytologist* Central Office.